PREPRINT UCRL-81088 Rev. 1

Lawrence Livermore Laboratory

LASER FUSION DIAGNOSTICS

LAMAR W. COLEMAN

AUGUST 16, 1978

Prepared for presentation at the 1978 International School of Plasma Physics, Varenna, Italy, September 4 - 16, 1978

LASER FUSION DIAGNOSTICS*

Lamar W. Coleman

University of California
Lawrence Livermore Laboratory
Livermore, California 94550

Abstract

The spatial and temporal scales of plasmas and processes characteristic of contemporary laser fusion target experiments have imposed special requirements for adequately diagnosing them. Particle and photon energies must be measured over a wide range. A diagnostic goal for laser fusion research is to be able, ultimately, to make measurements over the range of plasma parameters with spatial resolutions of 1 μm and 1 psec. Furthermore, the desired diagnostic technique should be capable of obtaining a complete data set on a single shot and should be amenable to direct interfacing to digital data systems for timely and efficient acquisition and analysis of experimental results. A variety of laser fusion diagnostic techniques in use, and under development, and their applications will be discussed.

High temporal and spatial resolution optical diagnostics of laser performance, energy balance, and ablatable plasma probing techniques will be reviewed. A variety of spatially, temporally and spectrally resolved x-ray diagnostics techniques and instruments will be discussed. Particular emphasis will be on high spatial resolution imaging techniques and applications and on high temporal resolution x-ray streak camera applications to exploding pusher target experiments. Finally, particle diagnostics and systems designed to diagnose target performance via rho-R and temperature measurements and techniques designed to determine the characteristics of compressed targets will be discussed.

*Work performed under the auspices of the U. S. Department of Energy by the Lawrence Livermore Laboratory under contract number W-7405-ENG-48.

INTRODUCTION

The detailed diagnosis of laser-target interaction experiments requires a variety of diagnostics techniques and systems capable of making measurements over a broad range of physical parameters with high spatial and temporal resolutions and which also conform to some system design and operational constraints. These requirements, goals and constraints are summarized in Table I. A wide range of physical parameters must be covered and an ultimate goal in being able to accurately diagnose laser target interaction experiments, is to be able to make broad variety of measurements of physical parameters with a spatial resolution of 1 μm and a temporal resolution of 1 ps and yet be able to cover the range of variables as indicated in Table I. As much as possible, we want to use multichannel diagnostic systems to avoid the necessity of having to do repetitive shots and taking "sampled" data that must then be put together to form a complete data set. Another requirement relates to interfacing diagnostics to computer aided data acquisition and analysis systems for fast and accurate acquisition, analysis, and display of data to enhance efficiency and interaction in the experimental program. There are a large number of types of measurements that are made and analyzed on laser fusion experiments, creating a need for proficiency in using the capabilities provided by interfacing diagnostics directly into digital data acquisition and analysis systems.

Various physical regions, shown schematically in Fig. 1, must be diagnosed during target irradiation experiments. The optical field from the laser irradiates the hollow glass microsphere target and creates plasma regions around the outside of the target in which the absorption and transport of energy around the target occurs. The pusher, the glass shell, is more dense, quite hot and is a copious emitter of x-rays. In the exploding pusher mode of target operation, characteristic of early fusion target experiments, the glass pusher heats up essentially uniformly, explodes and the inward exploding part of the shell compresses the fuel in the center of the target. In the ablative pusher mode of operation, the contemporary trend in target experiments, the outside of the shell is ablated off more gently and drives the inner and colder part of the shell inward against the fuel and compressing it at the center. Finally, there is the core, the compressed fuel region at the center of the target where the densities may vary over quite a large range depending on the details of the experiment, the target, and the nature of the fuel mixture in the center. In what follows we will try to approach the diagnostic problem from the outside in, beginning with a brief discussion of the ways in which we characterize the driving or input function, the energy from the laser that irradiates the target. Next some measurements that can be made to characterize the plasma atmosphere will be discussed, then diagnostics that relate to understanding the pusher implosion phase and finally some techniques for measuring the state of the compressed core target will be reviewed.

OPTICAL DIAGNOSTICS

An array camera (MacQuigg [1]) is used to characterize the laser spatial intensity distribution on the target. It is very important when performing target experiments to know the spatial and temporal distributions of energy in the laser pulse that irradiates the

target. In order to measure the spatial distribution a portion of the incident laser beam is directed to two pairs of mirrors. One of these pairs is closely spaced and of known reflectivities in order to provide a series of pulses of decreasing amplitude in a known ratio to one another. These pulses in turn arrive at another pair of mirrors wedged in an orthogonal plane and separated by a suitable distance so that the change in path length on each subsequent reflection is sufficient to shift the effective plane of focus a known amount in object space. This system is very carefully set up and calibrated so that the two-dimensional array of images that appear on the film represent a series of images at different intensities that correspond to intensity distributions in specific planes of the main beam where a target can be placed. Each column of images in this array, for example, consists of a series of time integrated pictures at the same equivalent object plane but attenuated relative to each other by the known factor. The known intensity step between pulses provides automatic calibration of the camera during the scanning and the evaluation of the data (MacQuigg [1]). Each row then represents a series of images at different equivalent planes. By analyzing images in the row corresponding to the target position the spatial profile of the optical energy incident on the target can be determined.

In order to measure the temporal history of the laser pulse hitting the target, we use a device known as an ultrafast streak camera (Korobkin [2]). The camera is an opto-electronic device in which the laser pulse (or other optical signal) to be measured is incident on a slit (nominally 25 μm high) which is then imaged onto the photocathode of an image converter tube. The electrons emitted from the slit shaped illuminated region of the photocathode are accelerated and focussed and then swept by means of a pair of deflection plates to which a suitable voltage pulse is applied to produce a streaked image on the phosphor screen at the back of the tube. That phosphor image is intensified by an image intensifier and then recorded on photographic film for analysis. In this way the temporal intensity versus time history of the incident optical signal is converted into a brightness, or film exposure, versus position image at the back of the camera. The time resolution capability of such cameras are in the 1 - 10 ps range with a total recording time in the range of about 0.5 - 2 nsec. From combined streak camera, array camera, and calorimeter (Ozarski [3], Gunn [4]) data, which provides total pulse energy accurately, a complete temporal and spatial distribution of the laser power incident on the target can be determined.

In conducting experiments not only is it important to know the details of the incident pulse that hits the target but it is also important to be able to measure the properties of whatever light is scattered or reflected from the target in order to understand the absorption, the energy balance and the energy partitioning occurring in the experiments. A number of measurements, similar to the types made on the incident beam, are made. A multiple array camera, a calorimeter, and a streak camera provide spatial and temporal details of the reflected light. A spectrograph (time integrated or time resolved) can be used to study the spectral properties of the reflected light. In addition, arrays of photodiodes and plasma calorimeters are placed internal to the target chamber to measure the angular distribution and amounts of scattered light and of the plasma blow off from the target. These types of measurements are essential for detailed studies to understand the partitioning of the energy and the efficiency of coupling of the laser beam to targets in a variety of target interaction experiments. The data from these measurements, together

with the results of the measurements on the light back-reflected through the lenses that focus the laser pulses onto the target then provide a detailed energy balance picture for a given experiment. A number of x-ray diagnostics instruments, which will be discussed later, are also placed at various positions around the target both within and outside of the target chamber.

In some experimental situations, a so-called box calorimeter is used to make very accurate measurements of the light absorption. In this case, the calorimeter has been devised to surround the target as completely as possible and intercept the nearly total amount of 1.06 μm light scattered during the irradiation. A transparent shield blocks ions, x-rays and target debris from the calorimeter absorber. Light reflected back through the entrance aperture or transmitted around or through the target and out a hole in the back of the calorimeter is recollimated and measured in separate calorimeters. This technique while providing accurate measurements suffers the drawback of completely surrounding the target and eliminates the use of many other possible diagnostics on a given experiment. It is therefore not used all the time but is used in cases where the highest possible accuracy measurements are required for absorption studies (Manes [5]).

ULTRAVIOLET PROBING

In order to understand more of the details of the energy absorption and transport in laser target interaction experiments, in addition to the energy balance and input pulse characterization measurements described earlier, it is also necessary to understand some of the details of the electron density distribution in the plasma atmosphere surrounding the target where the light is absorbed and energy transport occurs (Fstabrook [6]). One way to do this is to probe through the low density ($\sim 10^{21}$ e/cm^3) plasma atmosphere and measure the electron density distribution in that plasma via interferometry. The characteristics of the electron density distribution together with the knowledge of the characteristics of the input pulse can provide important information in describing and understanding the processes of absorption and transport that are taking place. The critical density for the 1.06 μm heating pulse, where absorption occurs, is 10^{21} electrons per cubic centimeter. In order to keep the refractive turning angle of the probe pulse to a small enough value that reasonable collecting and viewing optics can accept the rays probing up to that critical density, it is necessary to minimize the ratio of the probing pulse wavelength to the heating pulse wavelength and to keep the size of the plasma small (Attwood [7]). In our experiments we have chosen to use the fourth harmonic of the neodymium laser pulse that heats the target as the probing pulse. The spatial resolution of the interferometer used to measure the electron densities must be sufficently high to resolve small spatial scale lengths in the density distribution. Furthermore the probing pulse duration should be as short as possible compared to the heating pulse duration in order to obtain a "flash-stop action" photograph to freeze the motion of the electron density distribution that is characterized by an expansion velocity of ≈ 0.1 μm psec at times of interest when the interferograms are taken.

In an arrangement that is used at the Livermore Janus laser facility to obtain the short fourth harmonic diagnostic pulse used in ultraviolet plasma probing experiments, half of the output of the Janus laser oscillator is selected to be amplified in an auxillary

amplifier chain while the remainder of the oscillator pulse is amplified by the main laser and used to irradiate the target. The diagnostic pulse, after amplification, is then suitably conditioned and converted in a sequence of two crystals into the fourth harmonic (2660 Å) of the neodymium light. The pulse is shortened at this point by the frequency conversion process to about 15 ps in duration as compared to the 30 ps duration of the oscillator pulse and thus of the 1.06 μm heating pulse that irradiates the target. The 15 ps ultraviolet probing pulse passes through an adjustable time delay path so that the time of arrival of the diagnostic probe pulse at the target can be varied relative to the main heating pulse allowing interferograms to be obtained at different times during the interaction process. The reason for choosing this probe pulse generation technique is to maintain very precise synchronism between the heating pulse and the diagnostic pulse. Since these pulses are 30 ps and 15 ps respectively, precise synchronization between them is required in order to make adjusments on meaningful time scales for changing the probing time relative to the heating pulse. A holographic interferometer is used to obtain the electron density distribution data (Attwood [7]). The fourth harmonic probe pulse is split into object and reference beams, sent through a path equalizing arm, and propogated through the target chamber onto the holographic plate behind an appropriate interference filter. Double exposure holograms are made in order to obtain an interferogram which shows the line integral of electron density profiles at the time at which the exposure is made. Holographic interferometry was chosen because of its relative simplicity, stability, the fact that very high quality optical components are not required, and, of great importance, precise focussing of the interferometer is not necessary since the correct focus can be obtained in the reconstruction process to eliminate spurious fringes in the interferogram.

Results of measurements of this kind on 40 μm diameter hollow glass microsphere targets at about 10^{14} W/cm^2 irradiations were the first to directly show and verify the theoretically predicted effect of electron density profile steepening in the corona plasma produced at sufficiently high intensities by the ponderomotive force of the incident laser pulse (Attwood [8]). Density scale lengths shorter than 1.6 μm near critical density have been observed as shown in Fig. 2. An interferogram taken at the peak of the 30 psec target heating pulse is shown on the left and the Abel inverted axial electron density profile is shown on the right. This result provides experimental support of theories for absorption and transport processes based on the existence of the modified profile. Without the measurement capability providing 1 μm spatial resolution and 15 ps temporal resolution, direct measurement of this process would not have been possible. Interferometric measurements have also been made on thin planar plastic targets. In these cases the electron density distribution is much less uniform and there is evidence of a density cavity in the center of the plasma distribution. There is also evidence of small scale rippling near the critical density surface and a blurring of the outer fringes gives an indication that the blow-off velocity or the fringe motion velocity due to the changing density profile distribution is occuring faster in this case than it was on the microsphere targets. These observations of the contouring of the surface and the existence of structure on the critical density surface are important observations in providing experimental verification of models that have been used to calculate the characteristics of resonant absorption during laser irradiation processes (Estabrook [9]).

The existence and magnitudes of the magnetic fields generated in laser produced plasmas

will be important in developing an understanding of their effects on absorption and transport processes within the plasma (Kruer [10]). By probing through the plasma with the linearly polarized 2660 Å probe pulse, the angle of Faraday rotation of that plane of polarization due to fields can be measured. This data, together with the interferometric information on the size and density distribution of the plasma allows the magnitude of the magnetic field to be calculated. Magnetic field measurements have been made at Livermore and at other laboratories conducting laser fusion and laser plasma interaction research, recently producing a range of results with the highest fields approaching one megagauss under certain experimental conditions (Stamper [11]). The role of these fields in the laser target interaction and energy transport processes are not yet fully understood.

X-RAY MEASUREMENTS

Laser irradiated targets are copious x-ray emitters and diagnostics of these x-rays can provide detailed information in helping to understand and describe the processes occurring during the interaction and subsequent performance of the target. A typical time integrated x-ray spectrum obtained from a glass microballoon target irradiated with a neodymium glass laser covers the range from sub-keV to several tens of kilovolts. A portion of a typical time integrated spectrum (up to 10 keV) is shown in Fig. 3. X-ray spectral data is obtained on a single shot with a number of different instruments all of which are absolutely calibrated as indicated at the bottom of Fig. 3. X-ray fluences of 10^{16} - 10^{17} keV/keV in the few keV range of the spectrum are emitted in contemporary experiments on glass microshell targets. A variety of crystals are used for x-ray spectroscopy. These range from the lead myristate used at very low energies with moderate to low resolution to high resolution quartz crystals which can be used over a range of Bragg angles for energies as high as 10 keV. A great deal of the x-ray energy from target irradiation experiments resides in a portion of the spectrum below 1 - 2 keV. In order to understand fully the energy balance and energy partitioning it is necessary to measure the x-rays in that region of the spectrum. For this reason we have developed and begun to use detector systems, to diagnose the sub-keV spectral region (Slivinsky [12]). Basically, they are multichannel instruments, which provide spectral windows through the use of grazing incidence reflection to provide a high energy spectral cutoff, and transmission filters to provide the low energy cutoff to give fairly well-defined spectral channels or through the use of appropriate transmission filters alone. Spectral windows with widths of 200 - 300 eV in the $\gtrsim$ 0.2 - 1.0 keV range are obtained by these techniques. The fast windowless x-ray diodes used in these instruments have a response time of less than 100 ps. When coupled to suitably fast oscilloscopes, this combination can provide overall instrumental time resolution in the 150 psec range.

The higher energy portion of the x-ray spectrum above 2.5 - 3 keV is measured by a silicon pin diode array using K-edge transmission filter spectral definition (UCRL-50021-74 [13]). This is a technique that is being used for x-rays in the energy range of a few to about 10 keV in present experiments and provides sufficiently well defined channels to plot an accurate representation of the spectrum so long as the spectrum is falling with energy. This monotonic decrease is an important consideration in using the K-edge filter technique for obtaining good energy discrimination and accurate definition of the energy

windows covered by the different channels. As we progress to higher energy experiments using the larger laser facilities now coming on line, for example Shiva, we anticipate that the high energy x-ray spectrum may increase and that we will have difficulties with channel definition, and with interference and shielding of detectors. A filter fluorescer measurement technique, has been designed and is now being implemented for use on these systems. This is basically a system that will provide well-defined channels by using fluorescer foils together with suitable transmission filters in order to provide high energy x-ray spectral channels, and at the same time allowing effective separation from the target and shielding of the photomulitpliers or diodes.

The x-ray diagnostic techniques and systems reviewed to this point have all been basically for time integrated measurements. Now techniques that are used for making time resolved measurements on a picosecond time scale will be reviewed. An ultrafast x-ray streak camera has been developed for use in diagnosing laser plasma interaction experiments (McConaghy [14]). The basic concept of operation of this camera is very much the same as for the optical streak camera as discussed earlier. The main difference is that a suitable x-ray transmissive vacuum window (~ 25 μm Be) and an x-ray sensitive photocathode (~ 100 Å Au) have been substituted on the image converter tube. The time resolution of this camera is 15 ps, somewhat less than the optical camera because of the larger energy spread of the cathode photoelectrons in the x-ray case.

In one mode of use of this x-ray streak camera an array of K-edge filters is placed across the input photocathode slit so that the streak record contains time resolved information in a variety of x-ray spectral bins as determined by the particular sets of K-edge filters and prefiltering that are chosen (Attwood [15]). Several of the filters are used with multiple thicknesses to obtain intensity calibration information on the streak record. From the relative x-ray intensity as a function of time in the various spectral channels, time dependent temperature information can be obtained. Fig. 4 shows an example of such time resolved x-ray streak camera data. Data of this kind is valuable in studying the energy absorption, heating, and transport processes occurring in plasma interaction experiments.

Time-resolved x-ray emission histories measured with the x-ray streak camera can provide basic data on laser implosions of glass microsphere targets (Attwood [15]). The relative x-ray intensity plotted as a function of time for a particular energy channel in the multi-x-ray energy channel streak record shows a double-humped structure that can be explained in terms of the operation of these exploding pusher targets. Fig. 5 shows examples of time resolved x-ray emission histories for three different implosion experiments. The laser pulse incident on the target quickly heats the glass shell of the microballoon, its temperature rises and it begins to emit x-rays as indicated by an initial rise of the x-ray signal. At some point in this process, the shell explodes, its temperature and density drops, the x-ray emission drops, and there is a dip in the x-ray temporal history. Then the inward exploding part of the shell compresses the enclosed DT gas fuel, and eventually stagnates the center. The kinetic energy is converted into thermal energy at stagnation and a second burst of x-rays is emitted as evidenced by a second peak in the x-ray temporal profile. The temporal difference between the first peak, which corresponds to the heating of the shell, and the second peak, which corresponds to the stagnation of the imploded target shell at the center, can be interpreted as an implosion time. For the two identical

experiments in Fig. 5 the x-ray signatures are the same whereas for the lower power, lower performance shot a significant change in the profile and "implosion time" is evident. Data of this kind has provided important information for comparing and developing code calculations of target performance.

The x-ray streak camera just described is useful in the x-ray spectral range from about 1 keV to 20 or more keV. The low energy cutoff is determined by the thin beryllium vacuum window used to seal the image converter tube and provide the photocathode substrate. As was mentioned earlier, a significant part of the x-ray emission in these types of experiments resides in the region below 1 keV. A modification of the x-ray streak camera design which will allow us to significantly reduce the spectral threshold of the x-ray streak camera involves removing the beryllium vacuum window from the streak camera slit and replacing it with a very thin carbon substrate which will support the Au photocathode. This window will not withstand atmospheric pressure difference so the design of the camera system becomes physically more complex requiring pumping on both sides of the slit and careful control of operating conditions. In order to eliminate the higher energy x-rays and to be able to accurately measure the low energy portion of the spectrum, grazing incidence reflectors are used to direct the low energy x-rays of interest to the photocathode. Combinations of mirror materials and angles and transmission filters make simultaneous recording in several sub-keV channels possible. This capability greatly enhances our abilities for high time resolution measurements over a very broad range of the x-ray spectrum, down to the 100 eV range.

X-RAY IMAGING

To this point the discussion of x-ray diagnostics have related to diagnosing the low density plasma corona and the hot imploding glass shell of the target. The emphasis has been on spectral measurements and on time resolved measurements but there has been no imaging used to determine the spatial distribution of the x-ray emission from the target. X-ray imaging plays a very important role because it allows us to look at symmetries, evidence of compression, and to learn more about target dynamics and distributions of temperatures. Our goal is to be able to image x-rays with 1 μm spatial resolution and 1 ps temporal resolution for the purposes just described.

Pinhole cameras are very convenient instruments to use for x-ray imaging (Campbell [16]). They have been used widely for this purpose, they are good survey instruments, alignment is not a particular difficulty and the technique can provide resolution of a few microns with a few micron pinholes placed close to the target. X-ray microscopes based on grazing incidence reflection from appropriately curved surfaces offer advantages of high resolution at relatively large object distances to avoid problems from damage, especially in high energy experiments (Boyle [17]). The Kirkpatrick-Baez microscopes which are based on double reflections from orthogonal cylindrical mirrors, have so-far been the work horse of the x-ray imaging work at Livermore (Seward [18]). Fig. 6 is a schematic of a 4-channel Kirkpatrick-Baez x-ray microscope. They use a four channel configuration to obtain x-ray images in four different spectral bands in the 1-4 keV range with a spatial resolution of about 5 μm. Axi-symmetric microscopes comprised of hyperboloid-ellipsoid combinations, known as Wolter microscopes, offer potential for somewhat higher resolution with the advantage of having

much higher solid angle for collection of x-rays by about a factor of a thousand as compared with the Kirkpatrick-Baez microscope (Beyle [17]). This is important in applications where very high sensitivity and throughput is required. Another x-ray high resolution imaging technique is the use of zone plate cameras consisting of coded aperture microstructures in the form of Fresnel zone plates (Ceglio [19]). The technique of Fresnel zone plate coded aperture imaging is indicated schematically in Fig. 7. They are used in the shadowgraph mode and are particularly valuable for wavelengths shorter than those accessible by grazing incidence reflection microscopes. Newer techniques based on advanced zone plate structures and perhaps phase plate structures offer promise for efficient x-ray beam manipulation and focussing. Crystals can also be used in a mode to provide some energy selective imaging capabilities, which when combined with suitable probing sources, can result in effective systems for probing targets to measure density distributions, configurations, and perhaps dynamics.

An example of the type of data obtained from x-ray imaging is a set of time integrated images which show the effects on target implosion of focussing geometry and timing of the incident laser pulses. Analysis of such data provides a means of optimizing the irradiation conditions for most uniform heating and implosion.

In the zone plate coded imaging technique radiation from the source passes through a Fresnel zone plate coded aperture, and produces a shadowgraph of the zone plate on a suitable film plane. In order for this technique to work, sharp, crisp shadows must be cast by each "source point" in the object. This means that the technique can be used for any kind of source emission or radiation for which a suitable coded aperture, that is, one that is comprised of alternately opaque and transparent zones for the particular radiation to be imaged, can be built. Furthermore, the requirement that sharp shadows be cast means that diffraction cannot be tolerated in this application. For the case of x-rays, that requirement places limitations on the x-ray wavelength relative to the size of the zones. Once the shadowgraph has been formed, (the first step of this two-step process) in which each "point" in the source has created a unique shadow, so that the combined source has produced a distribution of overlapping shadow patterns on the film plane, a suitable laser can be used to reconstruct that coded image (the second step) to provide a real image of the original source distribution. In addition to having the capability of providing high spatial resolution, which is determined by the geometry of the system and the characteristics of the zone plate, the image is also tomographic. That is, the three dimensional characteristics of the source can be recovered by reconstructing images in different planes and recording them separately. This provides a distinct advantage over techniques in which the three dimensionality of the source distribution is not directly recoverable. The zone plate technique has been used to image thermal and supra-thermal x-rays from target irradiation experiments, (Ceglio [19]) and also to image alpha particles from the thermonuclear burn in the center of the compressed target (Ceglio [20]). A spatial resolution of 3 μm has been realized with this technique using a 100 zone free standing 5 μm thick Au zone plate with a 5 μm zone width. Details of the second application will be discussed further on.

TIME RESOLVED X-RAY IMAGING

The x-ray imaging discussed up until now has been time integrated, in other words, the

image recorded is integrated over the total duration of the x-ray output for a given experiment. It is very important to be able to do time resolved x-ray imaging to further understand the interaction and implosion processes. One technique that has been developed for time resolved x-ray imaging uses the ultrafast x-ray streak camera discussed earlier in conjunction with an x-ray pinhole camera (Attwood [21]). The technique is shown schematically in Fig. 8. The pinhole camera has high magnification (50X) in order to compensate for the spatial resolution limitation (≈ 100 μm) of the streak camera and still provide high resolution imaging of the target. The image of the target is carefully aligned onto the streak camera photocathode in such a way that the target diameter is placed on the photocathode slit. As the target is irradiated it begins to emit x-rays and the resulting streak camera record will then show the x-ray emission position across the diameter of the target as a function of time. In this way, since the x-rays being detected in these experiments are predominately those that come from the glass of the hot target wall, information on the implosion dynamics and the implosion time is obtained by the direct observation of the x-ray emission position with time from the streak record. A particular difficulty with implementing this technique is the very precise alignment that is required to ensure that the data obtained is correctly interpretable as just described. As can be seen by inspection of Fig. 8, a misalignment of the target image on the slit by one target radius will completely remove the image from the streak camera slit photocathode and no signal will be recorded. That means that since the compressed size of the target may be on the order of 10 μm, or so, that the alignment accuracy at the pinhole must be done to a micron level. An accurate optical technique has been developed in order to accomplish this alignment (Attwood [21], Attwood [22]). In order to obtain a high resolution x ray image, the size of the x-ray pinhole that images the target onto the streak camera must be kept very small; the diameter of the pinhole used is about 6 μm. Such a small pinhole produces severe diffraction at longer optical wavelengths so that optical alignment to the accuracy required would become for all practical purposes impossible. In order to solve this problem a dichroic pinhole is used (Attwood [22]). The x-ray pinhole, the small high resolution x-ray imaging pinhole, is laser drilled in a piece of glass doped with a high-Z element, either tungsten or tantalum. This glass is an effective x-ray absorber but it is optically transparent. A thin (12 μm thick) piece of gold with a 125 μm diameter pinhole in it is located relative to the tungsten glass so that the laser drilled pinhole is concentric with the 125 μm pinhole in the gold. The result is a composite system that provides a 125 μm optical pinhole for the alignment and a concentric 6 μm x-ray pinhole that provides the high resolution x-ray imaging. The technique has been used to effect system alignment to a few micron accuracy by centering the target in diffraction rings produced by apertures in the HeNe laser alignment system (Attwood [21]). Time resolved x-ray imaging data has been obtained with this technique on glass microsphere targets irradiated from two sides at the Janus laser facility. The space-time resolution in the images is 6 μm and 15 psec, respectively. Fig. 9 is an example of time resolved pinhole data obtained on a target experiment in which a glass microsphere target was irradiated simultaneously by pulses from two sides (the left and the right in the figures). The left hand photo is the actual streak record and the right hand figure shows the x-ray isoemission contours. From analysis of the x-ray streak records, implosion velocity profiles can be obtained. Velocities of $2 - 3 \times 10^7$ cm/sec have been measured directly for 70 μm initial diameter targets. This type of data is very important

in order to compare with the code calculations of target performance and has provided important experimental input parameters for target design calculations.

The next step in the development of the time resolved imaging technique of course would be the ability to obtain sequences of full, time resolved, two dimensional images instead of being limited to one dimension of spatial imaging because of the slit-shaped nature of a streak camera photocathode. Work is underway on the development of a technique capable of providing ultrafast two dimensional frames (Kalibjian [23]). This device makes heavy use of the technology developed for opto-electronic image converter based ultrafast streak cameras with some modifications in the basic operation to allow stationary frames to be obtained. Testing with a laboratory demountable prototype tube has demonstrated reconstructed frames each with a total time duration of about 125 ps comprised of a series of 10 - 15 psec time resolution elements. In addition to this very high time resolution it is also important that the spatial resolution in the image is quite high, better than 5 μm. This parameter is very important for meeting the requirement for very high spatial resolution imagery. The present status of this development is that two framing camera tubes are presently in fabrication, one with a visible photocathode that can be used in conjunction with a short pulse visible laser and other optical signals, to study short pulse operation and to calibrate the operation of the device. The second tube, with an x-ray photocathode, is for applications to target diagnostics. We anticipate being able to refine the operation of the devices to achieve frame times in the sub 100 picosecond range.

CORE DIAGNOSTICS

We now wish to turn to a discussion of some of the techniques used to measure to characteristics of the imploded core and the compressed fuel in laser fusion targets. The kinds of targets we are considering and working with basically consist of thin-walled glass microsphere targets filled with deuterium-tritium gas. As a target is heated and compressed an indicator of target performance is provided by the thermonuclear reaction products from the fuel. Neutrons, alpha particles, and protons can be detected and analyzed to determine some of the parameters achieved during the compression and heating of the fuel.

A variety of techniques have been used for measuring the yield from fusion target implosion experiments (Tirsell [24]). The number of neutrons, alpha particles, or in some cases protons, are usually measured by fluor-photomultiplier combinations, standard nuclear detector systems. The advantage of this kind of detector system is that it provides sufficient time resolution to provide time-of-flight separation for unambiguous signal identification, and high sensitivities can be obtained. For example, the time of flight separation of the 14-MeV neutrons relative to the x-rays produced from the target provides a convenient identification of the neutron signal. Absolute calibration of this kind of neutron detector is often difficult and in particular, accurate measurements in a high background of x-rays or other interfering signals can make accurate yield determinations quite difficult. For this reason we have begun to rely on nuclear activation as the main technique for measuring neutron yields. The principle activation scheme used in our experiments is based on the $^{63}Cu(n, 2n)^{62}Cu$ reaction with 14-MeV neutrons. ^{62}Cu decays by positron emission with a nearly 10-minute half-life. The 10-minute half allows ample time to retrieve a copper sample from the target chamber and the positron decay allows coincidence counting of the

two 511 keV annihilation gamma rays to realize low background counting. A copper disk is placed in proximity to the target and after the experiment it is retrieved and transported to thecoun.ing system. It is placed between a pair of sodium iodide crystals and coincidence counts in a standard nuclear counting system are recorded for a known time following the experiment. From the total number of coincidence counts recorded and the system calibration which has been determined on separate experiments at an accelerator, an value of the target neutron yield accurate to about 10% is obtained. This technique is particularly attractive because, for example, the $^{63}Cu(n, 2n)^{62}Cu$ reaction has a threshold at about 11 MeV and is insensitive to other radiations so that the activity obtained is due only to the 14-MeV neutrons. Other activation detection schemes, for example, Pb and O are also used. In order to extend the threshold for neutron activation detection to a level of about 10^4 neutrons we have used a lead activation scheme. By placing the detector very close to the target high sensitivity can be obtained. Because of the short half-life, 0.8 sec, the counting of the activated Pb is done in place. A dioxane detector (dioxane is a liquid scintillator material) which depends on an np cross section in oxygen, has also been built and offers advantages similar to the lead counter. However as the basic technique for yield diagnostics, for sufficiently high yield, ($\gtrsim 10^8$) we continue to rely on the copper because of the minimal background problem inherent in coincidence counting techniques and because of the lack of other radiation interference problems.

In addition to measuring the total yield in target experiments another extremely important parameter is the ion temperature of the reacting fuel. In one technique a target is used in which the deuterium fuel also contains ^3He. Because of the differences in the temperature dependence of the reaction cross section for the DD reaction (which produces 3 MeV protons) as compared to the the D^3He reaction (which produces 14.7 MeV protons), measuring the ratio of the protons produced by the DD fusion reaction as compared to the D^3He fusion reaction provides an estimate of the temperature of the reacting fuel. The ratio of those cross sections is a fairly strong function of temperature. Experiments with this technique have been done successfully and have succeeded in measuring ion temperatures in the range of 6 - 8 keV (Slivinsky [25]).

Because a laser fusion target is an excellent spatial and temporal point source it is possible to perform time of flight spectral measurements in order to obtain energy spreads and therefore temperatures of the reacting ions in the fuel. The particles emitted from the target have an energy spread characteristic of the temperature in the reacting fuel because of the reacting ion velocity distribution. This will be true as long as the target is "thin" to the emitted radiation. After a suitable flight path this spread in energy results in a measurable spread in arrival times at a detector. Knowing the detector response, the energy spread can be obtained from the time spread of the signal and the corresponding ion temperature of the reacting fuel can then be determined.

Alpha particle time-of-flight measurements have been made at Livermore and elsewhere. These were the first measurements which confirmed the thermonuclear nature of the reactions occurring in the compressed core of a laser irradiated target (Slivinsky [26]). Because of the lower energy and velocity of the DT alpha particles as compared to the neutrons, an alpha particle spectrometer can be shorter and more sensitive than a 14-MeV neutron spectrometer with the same resolution. It can be used at lower yields, greater than about 5×10^5, and sufficiently low density targets ($\lesssim 10^{-1} g/cm^2$). We have implemented a

neutron time of flight spectrometer on the Argus facility. Using a neutron flight path of 45 m (Lerche [27]). Neutron time of flight data obtained on Argus experiments that produced about $\gtrsim 10^8$ neutrons have measured reaction temperatures in the range 4 - 8 keV. Fig. 10 shows an example of Argus neutron time of flight spectral data. The error bars are determined by the number of neutrons detected in each resolution interval. The distribution in neutron energy around the mean energy of 14 MeV has a FWHM of $\sim$ 400 keV for this data. In order to increase the energy resolution of a time of flight spectrometer it is necessary to improve the time response of the detector or increase the flight path to increase the time spread for a given energy spread, or both. The neutron time of flight spectrometer recently built at the Shiva facility at Livermore is capable of higher resolution because of a longer flight path. The flight path for the Shiva system is 125 m as compared to the 45 m on Argus. The same type of detectors are used. The ultimate resolution of the Shiva system, given a sufficient number of neutrons from the target, 1×10^{11}, is 25 keV.

Another very important diagnostic on target experiments is to be able to measure the spatial distribution of the thermonuclear reaction products in order to determine information about the size (density) and symmetry of the compressed fuel in the target. The alpha particles have been imaged with a pinhole camera (Slivinsky [28]). Earlier, the technique of zone plate coded imaging was discussed with reference to its applications to x-ray . This technique has also been used to image the alpha particle emission from the compressed burning DT fuel in a target (Ceglio [20]). The emitted alpha particles cast shadows through a 5 μm thick, 100 zone Au Fresnel zone plate. The recording medium, in this case as in the pinhole case, is a cellulose nitrate polymer track detector. It is very important to have sufficient discrimination so that the other emissions from the target do not produce an image in the recording medium which can be confused with that produced by the alpha particles. A filter foil of 0.3 mil beryllium is used in front of the recording medium. Discrimination experiments have been performed which show that this arrangement is sufficient to ensure that the developed image on the cellulose nitrate is due only to the alpha particles. The alpha particles deposit energy and produce damage tracks in the cellulose nitrate. When the 6 μm thick cellulose nitrate is properly etched with sodium hydroxide, the alpha particle damage tracks produce pinholes completely through the film. Other radiations do not produce pinholes of that type and therefore the resulting pattern of pinholes is due to the alpha particles. In order to reconstruct the zone plate alpha particle image the cellulose nitrate film is contact printed through a suitable filter onto photographic emulsion to transform the pinhole array to a photographic density distribution which is then used as the coded image for reconstruction with a laser. The resolution of the first order reconstructed image is about 10 μm. The measured total extent of the alpha particle emission region is about 30 μm. This data is unambiguous in providing a clear representation that the source of DT alpha particle emission is from the central region of the compressed target.

An improvement in the zone plate shadow casting technique has been the realization and the demonstration that the images can be reconstructed in higher order (Gur [29]). The data discussed above were reconstructed in the first order with a resolution of about 10 μm. By reconstructing in a higher order, for example the third order, higher resolution in the image is realized. The principal difficulty to be overcome in implementing high order reconstruction is that the signal to noise ratio decreases at higher orders and it has been necessary to experimentally develop the appropriate optical techniques to obtain sufficiently

high signal to noise ratio images in the higher orders. The same alpha particle data discussed above that was reconstructed in first order with 10 μm resolution has also been reconstructed in third order with a resolution of 3 μm and shows some image structure not evident in the first order image. Fig. 11 summarizes an alpha particle imaging result and shows the isoemission contours for the first order (10 μm resolution) image at the lower left and the third order (3 μm resolution) alpha particle image of the compressed target at the lower right. The diameter of the alpha particle emission region measured from the third reconstructed image is about 20 μm. Since the original target diameter was 86 μm, this result corresponds to a volume compression of about 80. This technique for compression measurement does not rely on the interpretation of the origin of x-rays as is necessary in evaluating x-ray pinhole or microscope images in terms of fuel compression. The higher order reconstruction is most useful if the wavelength of the radiation being imaged is short enough that diffraction effects have not already limited the resolution available in the shadowgraph. This does not puse a limitation for the alpha particle images. However for x-ray applications the diffraction effects can limit the improvement accessible by higher order reconstruction.

Most of the experiments that have been discussed up until now have been done with so-called exploding pusher targets. As discussed earlier, with this type of target a short laser pulse uniformly heats a thin glass shell target which then explodes. The inward exploding part, drives against the fuel compressing it. This type of performance, although valuable for the early stages of laser fusion target implosion research, must be altered toward experiments with ablatively driven targets capable of compressing the fuel to higher densities. These types of targets are scalable to the levels of performance that are necessary to begin to study the achievement of conditions of thermonuclear performance that can lead to possible breakeven conditions for laser fusion (Nuckolls [30]). In beginning to experimentally study the performance of targets of this type we enter a regime where yields and temperatures will be lower than with current exploding pusher targets. In fact yields will be low enough initially that some of the techniques already discussed for diagnosing the state of the compressed fuel at the core of the target cannot be applied. As higher densities are achieved the alpha particle and charged particle diagnostics cannot be used because the alpha particles will no longer escape the target and other charged particles start to suffer significant scattering and energy loss in passing through the dense target walls. Among other techniques that have been studied and implemented for diagnosing this kind of experiment is the possibility of seeding the DT fuel with a suitable material which can emit characteristic x-rays whose properties can be measured to determine information about the state of the compressed core (Yaakobi [31]). With a suitable spectrograph the x-ray spectral lines from neon, for example, can be studied and from the broadening and shape of these lines information on the temperature and density in the core can be deduced.

It is also possible to obtain images with the radiation emitted by a material doped into the fuel. (Slivinsky [32]). Argon, for example, can be doped into the fuel and using the 3.1 keV line emission, a suitably placed quartz crystal can transfer the width of the emitting argon region onto a suitable film plane. The technique can provide a resolution of the order of 10 μm presently. This level of resolution is sufficient to be able to obtain a value for compressed density to within a factor of two for about a 10 μm core size. Although this technique has not yet been demonstrated in an actual implosion experiment,

preliminary experiments are underway to test the system and the survivability of the components in the environment of target experiments.

Another technique that is being developed for use as a density diagnostic is radiochemistry (Mayer [33]). In this technique the 14-MeV neutrons generated by the reaction of the DT fuel pass through the glass wall of the target. The glass contains about 25% composition of ^{28}Si. The 14-MeV neutrons produce ^{28}Al by the $^{28}Si(n, p)^{28}Al$ reaction. The ^{28}Al decays with a half-life of 2.24 minutes emitting a gamma ray and a beta particle. By conducting an implosion experiment and then suitably collecting and counting a known amount, the target debris, the number of ^{28}Al atoms that were produced can be determined. With an independent measurement of neutron yield, then information can be obtained about $(\rho r)_p$, the density thickness product of the compressed glass shell at the instant of neutron production. From this information calculation can provide information on the density times the radius product, the $(\rho r)_F$ of the compressed fuel. A number of experiments have been conducted to evaluate this technique. Calibration experiments using a ^{24}Na tracer technique have verified that as much as 80 - 90% of the target material can be collected in large aspect ratio cylindrical collectors. A large volume coincidence counting system has been demonstrated with a counting efficiency of 40% and a background of about 0.5 counts per minute. This means that for a $(\rho r)_p$ of 10^{-2} grams per square centimeter and a neutron yield of 10^7, twenty beta-gamma coincidence counts can be obtained in a five minute interval with a background in the 15 - 20% range. These values represent the current level of capability for this radiochemistry technique. More complicated radiochemical schemes can be used for the diagnosis of very much more complex future targets. By suitably seeding each of the materials used to make up a multi-shell target, a variety of neutron induced reactions will allow measurement of the ρr's of the various shells by collecting the target debris and counting the decays of the various activations.

SUMMARY

In summary, Table 2 shows the current status of the capability of laser fusion diagnostics. Optical and infrared streak cameras provide time resolution measurement capability of less than 10 ps, while x-ray streak cameras provide 15 ps time resolution in the range of about 0.1 - 20 keV presently. Time integrated spatial resolutions of 1 μm are provided with a variety of optical techniques. Ultraviolet holographic interferometry has measured electron densities above 10^{21} cm^{-3} with about 1 μm spatial resolution and 15 ps temporal resolution. X-ray microscopes provide 3 μm time integrated resolution and the 15 psec time resolution x-ray streak pinhole camera has 6 μm spatial resolution Development of an ultrafast framing camera has thus far provided 50 μm spatial resolution with 125 ps frame duration. The third order reconstruction of zone plate images has provided 3 μm resolution for alpha particles. Finally, the new Shiva neutron spectrometer increases the energy resolution capability of that technique to 25 keV for 14-MeV neutrons. These combined capabilities provide a unique set of diagnostics for the detailed measurement of the interaction of laser light with targets and the subsequent performance of those targets.

Acknowledgement

The work described here represents the results of the work of a large number of people in various disciplines. Without the dedication and committment to accomplishment on the part of these many people, much of what has been reported here could not have been. References to original work in the technical topics are contained in the bibliography.

References

1. D. R. MacQuigg, "Argus Beam Diagnostics" 1976 LLL Laser Program Annual Report, p. 3-37 UCRL-50021-76.
2. V. V. Korobkin and M. Ya Schelev, Proc. 8th Int'l. Cong. on High Speed Phtogography, Stockholm; John Wiley and Sons, 1968, p. 36.
   D. J. Bradley, B. Liddy, and W. E. Sleat, Opt. Comm. 2, 391 (1971).
   M. Ya Schelev, M. C. Richardson and A. J. Alcock, Appl. Phys. Lett. 18, 354 (1971).
   S. W. Thomas, G. R. Tripp and L. W. Coleman, Proc. 10th Int'l. Cong. on High Speed Photography, Nice, France, 1972, p. 127.
   S. W. Thomas, J. W. Houghton, G. R. Tripp and L. W. Coleman, Proc. 11th Int'l. Cong. on High Speed Pho'ography, London, U.K., 1974 p. 101.
3. R. G. Ozarski "Beam Diagnostics" 1976 LLL Laser Program Annual Report p. 2-155, UCRL-50021-76.
4. S. R. Gunn "Calorimetric Measurements of Laser Energy and Power", Journal of Phys. E: Scientific Instruments 6, p. 105, 1973.
   S. R. Gunn "Volume-Absorbing Calorimeters for High-Power Laser Pulses", Rev. Sci Instrum. 45, p. 936, 1974.
   S. R. Gunn and V. C. Rupert "Calorimeters for Measurement of Ion, X-rays, and Scattered Radiation in Laser-Fusion Experiments", Rev. Sci. Instrum. 48, p. 1375, 1977.
5. K. R. Manes, et al, "Polarization and Angular Dependence of 1.06 um Laser Light Absorption by Planar Plasmas", Phys. Rev. Lett., 39. p. 281, 1977.
6. K. G. Estabrook, E. J. Valeo, and W. L. Kruer, Phys. Fluids, 18, 9, Sept. 1975, pp. 1151-1159.
   K. Lee, D. W. Forslund, J. M. Kindel and E. L. Lindman, Phys. Fluids, 20, 1, January 1977, pp. 51-54.
7. D. T. Attwood, "Ultraviolet Probing of Laser-Produced Plasmas with Picosecond Pulses. Proc. 12th Int'l. Cong. on High Speed Photography. SPIE, Vol. 97, Bellingham, Wash. p. 413.
   D. T. Attwood and L. W. Coleman, "Microscopic Interferometry of Laser Produced Plasmas", App. Phys. Lett. 24, p. 408, 1974.
8. D. T. Attwood, D. W. Sweeney, J. M. Auerbach, and P. H. Y Lee, "Interferometric Confirmation of Radiation-Pressure Effects in Laser-Plasma Interactions", Phys. Rev. Lett. 40, p. 184, 1978.
9. K. G. Estabrook, E. J. Valeo, and W. L. Kruer, "Two-Dimensional Relativistic Simulations of Resonance Absorption", Phys. Fluids 18, p. 1151, 1975.
10. W. L. Kruer and Kent Estabrook, "Laser Light Absorption Due to Self-Generated Magnetic Fields", Phys. Fluids 20, p. 1688, 1977.
11. J. A. Stamper and B. H. Ripin, Phys. Rev. Lett. 34, p. 138, 1975.
    J. A. Stamper, E. A. McLean, and B. H. Ripon. "Studies of Spontaneous Magnetic Fields in Laser Produced Plasmas by Faraday Rotation", Phys. Rev. Let. 40, pp. 1177-1181, 1978.
12. V. W. Slivinsky, H. Kornblum, and G. Tirsell, "Sub-keV, Sub-nanosecond X-ray Measurements on Laser Fusion Targets". To be published Nuc. Insts. and Meth.

13. "K-edge Filter Detectors", Lawrence Livermore Laboratory 1974 Laser Program Annual Report, p. 310, UCRL 50021-74.

14. C. F. McConaghy and L. W. Coleman, "Picosecond X-ray Streak Camera", App. Phys. Lett. 25, p. 268, 1974.

15. D. T. Attwood, L. W. Coleman, J. T. Larsen and E. K. Storm, ,"Time Resolved Spectral Studies of Laser Compressed Targets, Phys. Rev. Lett. 37, 499 (1976).

16. P. M. Campbell, G. Charatis, and R. Monty, "Laser Driven Compression of Glass Microspheres", Phys. Rev. Lett. 34, p. 74, 1975.

17. Michael J. Boyle and Harlow G. Ahlstrom, "Imaging Characteristics of an Axisymmetric, Grazing Incident X-Ray Microscope Designed for Laser Fusion Research". To be published Rev. Sci. Instrum. 1978.

18. F. Seward, et. al., "Calibrated "Four Color" X-Ray Microscope for Laser Plasma Diagnostics", Rev. Sci. Instrum., Vol. 47, No. 4 April 1976.

19. N. M. Ceglio, et. al., "Zone Plate Coded Imaging (ZPCI) of Laser Compressed Targets", Bull. Am. Phys. Soc., Vol. 21, No. 9, p 1078, October 1976.
N. M. Ceglio, Journ. Appl Phys. 48, p. 1563, 1977.

20. N. M. Ceglio and L. W. Coleman, "Spatially Resolved Emission From Laser Fusion Targets", Phys. Rev. Lett. 39, p. 20, 1977.

21. D. T. Attwood, L. W. Coleman, M. J. Boyle, J. T. Larsen, D. W. Phillion and K. R. Manes, "Space-Time Implosion Characteristics of Laser-Irradiated Fusion Targets", Phys. Rev. Lett., 38, 282 (1977).
D. T. Attwood, "Time Resolved X-ray Pinhole Photography of Compressed Laser Fusion Targets". Proc. 12th Int'l. Cong. on High Speed Photography. SPIE, Vol. 97, Bellingham, Wash. p. 325.

22. D. T. Attwood, B. W. Weinstein and R. F. Wuerker "Composite X-ray Pinholes for Time-Resolved Microphotography of Laser Compressed Targets", App. Opt. 16, p. 1253, 1977.

23. R. Kalibjian, "Optical/X-ray Framing Camera Tube". Proc. 12th Int'l. Cong. on High Speed Photography. SPIE, Vol. 97, Bellingham, Wash. p. 269.
R. Kalibjian, "A 100-ps Framing Camera Tube". To be published Rev. Sci. Instr., July, 1978 - (UCRL-79915).

24 K. G. Tirsell, R. A. Lerche, L. W. Coleman and V. W. Slivinsky, "Yield Measurements for D-T Laser Fusion Experiments". Submitted to Jour. App. Phys. (UCRL-80619).

25. V. W. Slivinsky, et al., "Implosion Experiments with D_2, ^3He Filled Microspheres", Jour. App. Phys., 49, p. 1106, 1978.

26. V. W. Slivinsky, et al., "Measurement of the Ion Temperature in Laser Driven Fusion", Phys. Rev. Letts., p. 1083, 1975.

27. R. A. Lerche, L. W. Coleman, J. W. Houghton, D. R. Speck and E. K. Storm, "Laser Fusion Ion Temperatures Determined by Neutron Time-of-Flight Techniques", App. Phys. Lett. 31, p. 645, 1977

28. V. W. Slivinsky, et al., "Pinhole Imaging of Laser Produced Thermonuclear Alpha Particles", App. Phys. Lett. 30, p. 555, 1977.

29. J. Gur and J. M. Forsythe, "Optical Simulation of a Technique for Obtaining Submicron Resolution of X-ray Images in Laser Pellet Compression Experiments", Appl Optics, 17, p. 1, 1978.

N. M. Ceglio, "Third Order Reconstruction of Zone Plate Coded Images for Improved Resolutions", Bull. Am. Phys. Soc., 22, p. 1196, 1977

30. J. Nuckolls, L. Wood, A. Thiessen and G. Zimmerman "Laser Compression of Matter to Super-High Densities; Thermonuclear (CTR) Applications", Nature, 239, pp. 139-142, Sept 1972.

J. Nuckolls, J. Emmett and L. Wood, "Laser-Induced Thermonuclear Fusion", Phys. Today 26, pp. 46-53. Aug. 1973.

J. Emmett, J. Nuckolls, and L. Wood, Sci. Amer. 230, pp. 24-37, June 1974.

31. B. Yaakobi, D. Steel, E. Thorsos, A. Hauer, and R. Perry, "Direct Measurement of Compression of Laser Imploded Targets Using X-Ray Spectroscopy", Phys. Rev. Lett., 39, p. 1526, 1977.

J. M. Auerbach, Y. L. Pan, V. W. Slivinsky and S. S. Glaros, "Experiments on Super Liquid Density Implosions of Laser Fusion Targets", Bull. Am. Phys. Soc. 21, p. 1140, 1976.

J. M. Auerbach, et al., "Neon Line Emission from the Fuel Core of Compressed Laser Fusion Targets". In preparation for submission to Plasma Phys.

32. V. W. Slivinsky, G. R. Leipelt, and J. D. Eckels, "A Crystal Spectrograph for Imaging High Density Targets", Bull. Am. Phys. Soc., 22, p. 1112, 1977.

33. F. J. Mayer and W. B. Rensel, "Plastic Bubbles and Tamper ρR Measurements for Laser-Driven Fusion Experiments", Jour. Appl. Phys., 47, p. 1491, 1976.

E. M. Campbell, et al., "Radio Chemistry As A Diagnostics in Laser Fusion Experiments" Bull. Am. Phys. Soc. 22, p. 1113, 1977.

Figure Captions

Figure 1. Schematic diagram of a laser heated hollow glass microsphere target showing characteristic regions to be diagnosed and the corresponding ranges of electron densities.

Figure 2. Holographic interferogram of laser irradiated hollow glass microsphere target (left) showing electron density produced fringes. Abel inverted axial electron density profile (right) shows steepened profile in the range 0.25 x 10^{21} to over 10^{21} e/cc.

Figure 3. Time integrated x-ray spectrum in the sub-10 keV range from glass microsphere target. A summary of instruments used to measure various regions of the spectrum is given at the bottom.

Figure 4. Time resolved (15 psec) x-ray emission from laser irradiated Au disk. The left hand set of curves show x-ray streak camera recorded intensity profiles in various spectral regions determined by K-edge filters as indicated in the inset table. Laser pulse length was 242 psec FWHM. The right hand set of curves are derived from the data at the left and show spectral shapes at different times. The various times and the thermal and suprathermal temperatures deduced from the slopes of the curves are given in the inset.

Figure 5. X-ray intensity profiles from three imploding glass microsphere target experiments. The first intensity peak corresponds to the initial heating of the target pusher and the second peak is produced by stagnation of the imploded target material. The time between peaks is interpreted as an implosion time.

Figure 6. Schematic diagram of a four-channel Kirkpatrick-Baez x-ray microscope. Rays that are reflected from both cylindrical surfaces form an image at the film plane a spatial resolution of about 5 μm is realized.

Figure 7. Concept of Fresnel zone plate coded aperture imaging. In the encoding step, emission from the source casts shadows of the zone plate to form the shadowgraph which is recorded on suitable film. In the second step the image is decoded or reconstructed by illuminating the shadowgraph with a suitable source to exploit the diffracting properties of the shadowgraph.

Figure 8. Schematic representation of the time resolved x-ray pinhole imaging technique. Space-time resolutions of 6 μm and 15 psec have been achieved with this technique.

Figure 9. Result of a time resolved x-ray pinhole imaging measurement on a 69 μm diameter hollow glass microsphere target implosion experiment. The target was irradiated by simultaneous laser pulses from the left and the right. The left hand photo is the actual streak camera record. The right hand figure is the isodensity map. The dashed lines representing the target implosion velocity profile and subsequent disassembly follow the peaks of x-ray emission intensity.

Figure 10. Example of neutron time of flight spectral data obtained on an experiment at the Argus laser facility.

Figure 11. Alpha particle image results obtained with the zone plate coded imaging technique. The lower left and lower right isodensity maps show the alpha particle images with 10 μm and 3 μm spatial resolution, respectively.

TABLE 1

DIAGNOSTICS REQUIREMENTS

10^{16} $cm^{-3} \leqslant n \leqslant 10^{26}$ cm^{-3}

1 eV $\leqslant h\nu \leqslant$ 500 keV

1 eV $\leqslant E \leqslant$ 14 MeV

1 μm $\leqslant \Delta x \leqslant$ 1 cm

1 psec $\leqslant \Delta t \leqslant$ 20 nsec

Data obtained on a single shot basis

Compatible with computer aided data acquisition

Table 2

CURRENT STATUS OF LASER FUSION DIAGNOSTICS

Δt = 6 psec (infra-red)

= 15 psec (x-ray)

Δx = 1 μm (visible, ultra violet; time integrated over pulse duration)

= 3 μm (x-ray; time integrated)

= 6 μm (x-ray; 15 psec time resolution)

= 50 μm (125 psec, full frame)

= 3 μm (α particles, ions)

$100\ eV \leq h\nu \leq 100\ keV$ (time integrated)

$100\ eV \leq h\nu \leq 20\ keV$ (15 psec time resolution)

$10^{16}\ cm^{-3} \leq n_e \leq 10^{21}\ cm^{-3}$ ($\approx$15 psec exposures)

$\Delta(h\nu) = 1\ eV$ at 1 keV

$\Delta E = 25\ keV$ for 14 MeV neutrons, 3.5 MeV alphas

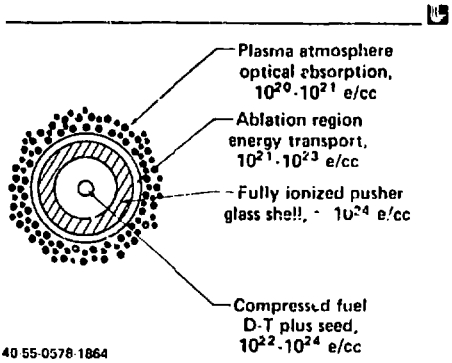
Plasma atmosphere
optical absorption,
10^{20}-10^{21} e/cc
Ablation region
energy transport,
10^{21}-10^{23} e/cc
Fully ionized pusher
glass shell, ~ 10^{24} e/cc
Compressed fuel
D-T plus seed,
10^{22}-10^{24} e/cc
40-55-0578-1864

Fig. 1

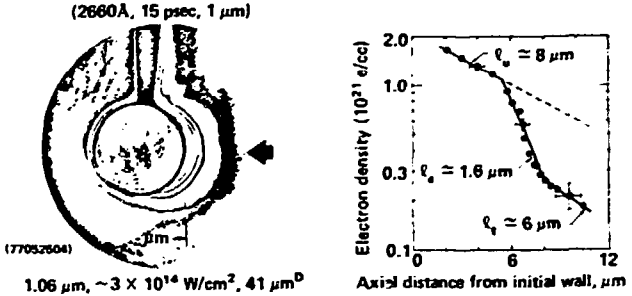
(2660Å, 15 psec, 1 μm)
(77052604)
μm
1.06 μm, ~3 × 10^14 W/cm^2, 41 μm^D
Electron density (10^21 e/cc)
2.0
1.0
0.3
0.1
0
6
12
ℓ_n ≃ 8 μm
ℓ_e ≃ 1.6 μm
ℓ_i ≃ 6 μm
Axial distance from initial wall, μm

Fig. 2

COMPOSITE X-RAY SPECTRUM, FROM FOUR INSTRUMENTS, FOR A GLASS MICROSPHERE TARGET (140 μm DIAMETER)IRRADIATED BY THE ARGUS LASER WITH A 535J, 187 ps GAUSSIAN PULSE

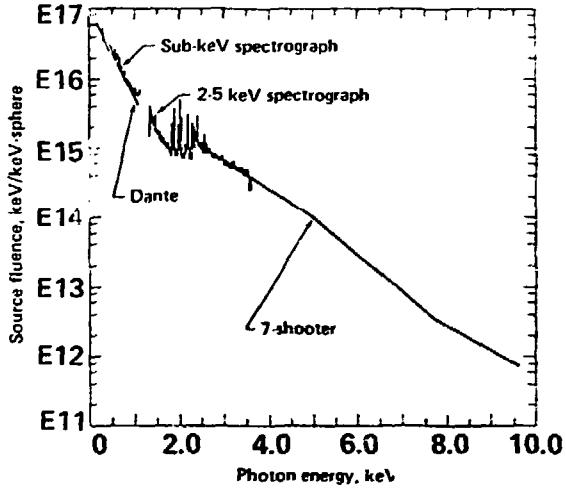

	Instrument	Description	Coverage
	Dante	Filter/reflector discrimination, fast XRD	0.2-1.1 keV in 3 ch's
	Sub-keV spectrograph	Lead myristate xtal diffraction, VUV film	0.32-1.0 keV, 10 eV resolution
	2-5 keV spectrograph	RAP xtal diffraction, no-screen film	1.4-4.2 keV, 2-3 eV resolution
20-90-0777-1508	Seven shooter	Filter discrimination, PIN diode	2.5-3.0 keV in 6 chls

Fig. 3

TIME-RESOLVED X-RAY EMISSION AND X-RAY SPECTRA OF Au-DISK

Shot #37070712: 357 J/242 ps, 2.82 × 10^{15} W/cm^2

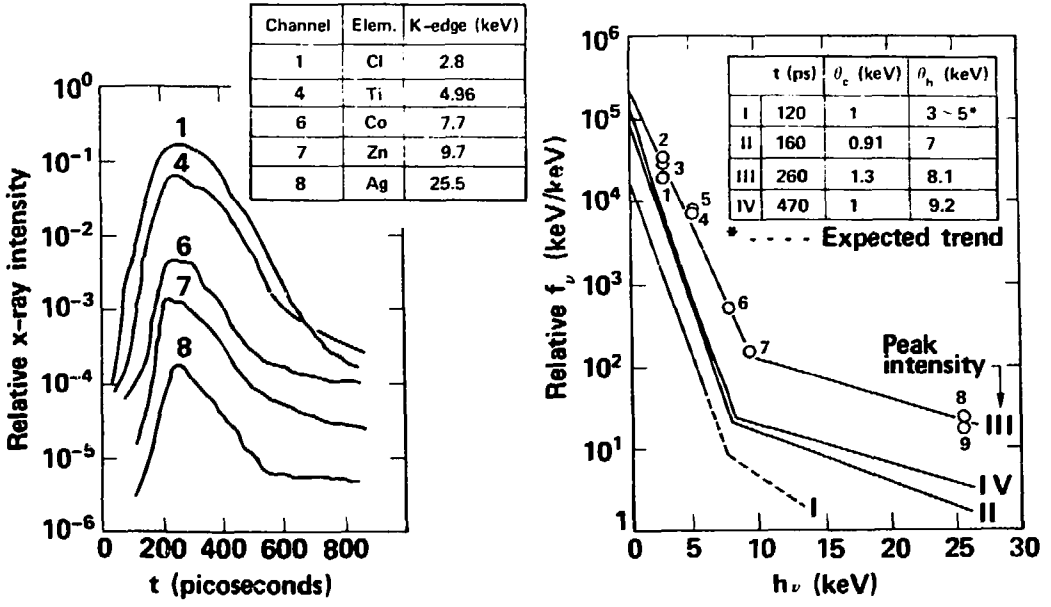

20-60-0877-1540

Fig. 4

X-RAY TEMPORAL SIGNATURE AS A FUNCTION OF LASER POWER

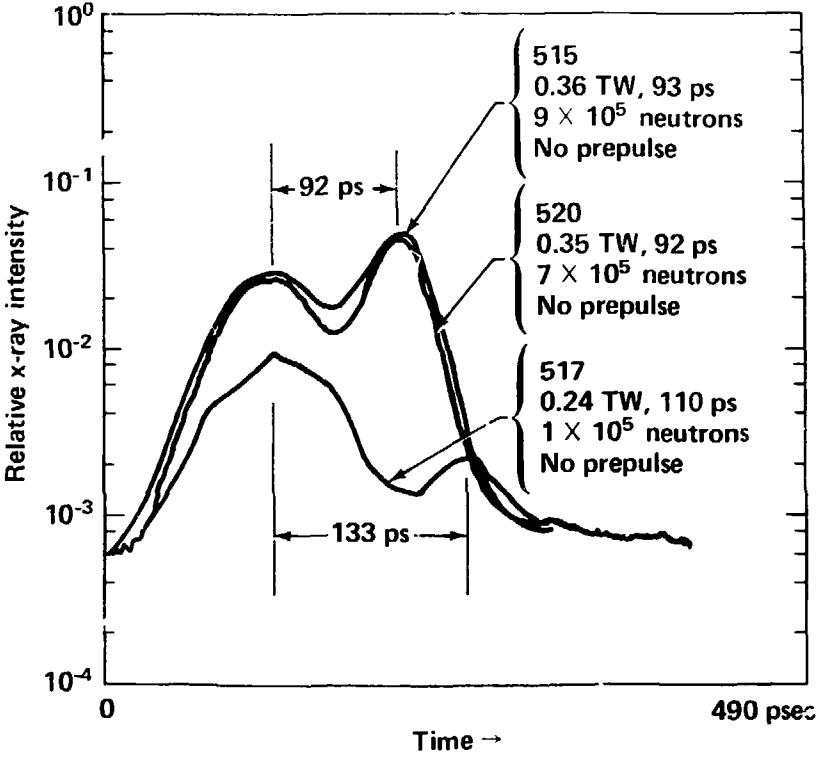

Fig. 5

SIMPLE 4-CHANNEL X-RAY MICROSCOPE

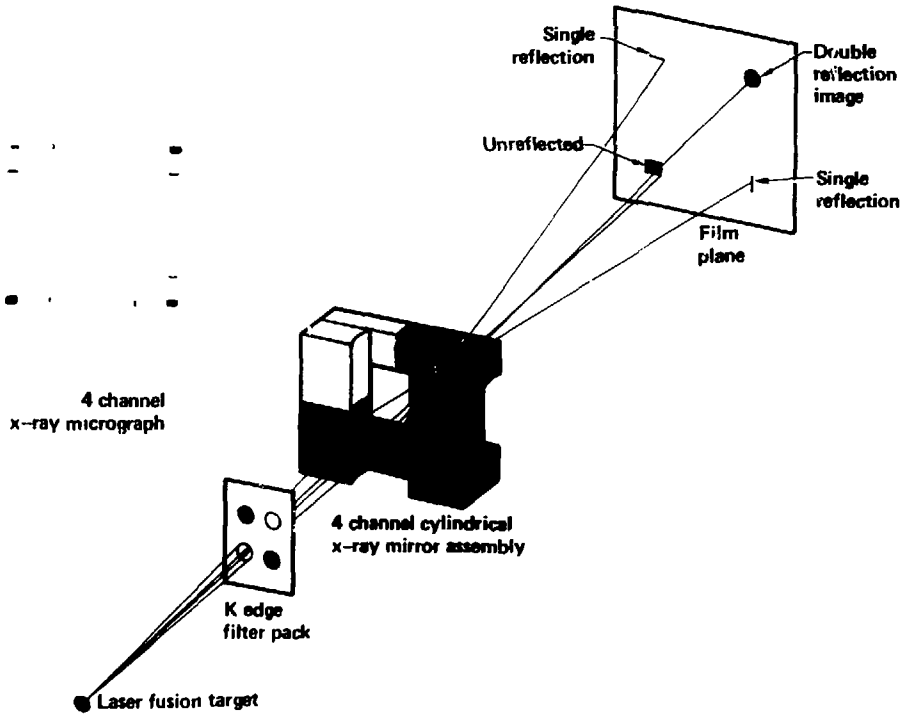

20-50-0877-1847

Fig. 6

ZONE PLATE CODED IMAGING (Technique:)

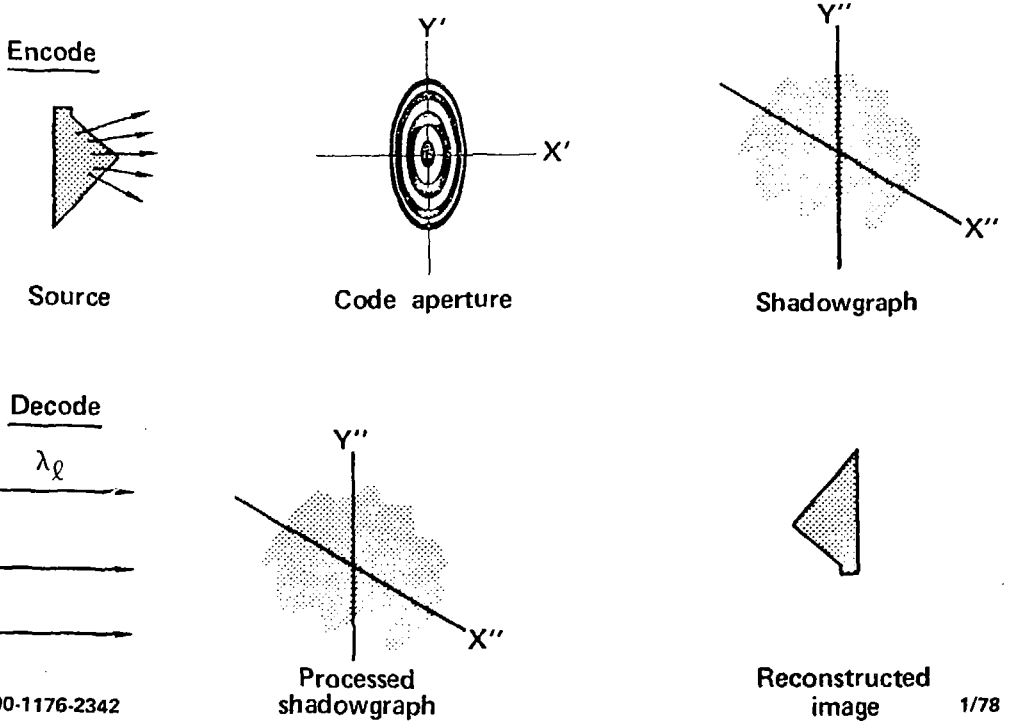

40-90-1176-2342

1/78

Fig. 7

TIME RESOLVED X-RAY PINHOLE PHOTOGRAPHY

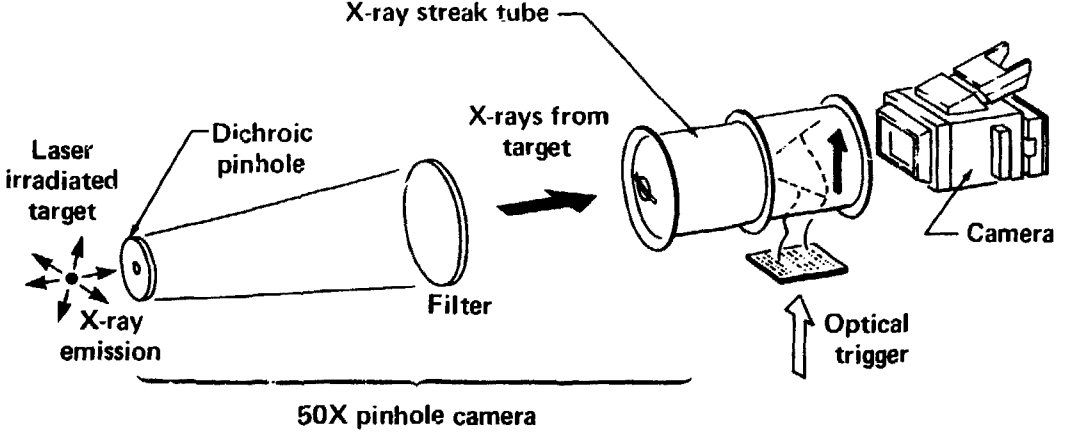

Fig. 3

ASYMMETRIC TWO-SIDED TARGET IMPLOSION

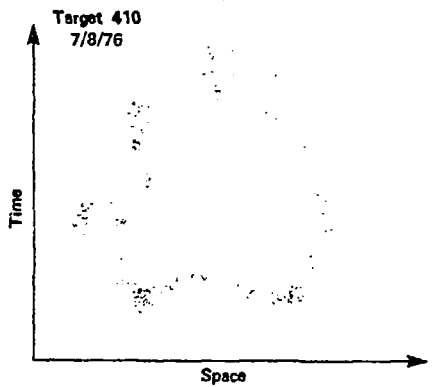

(a)

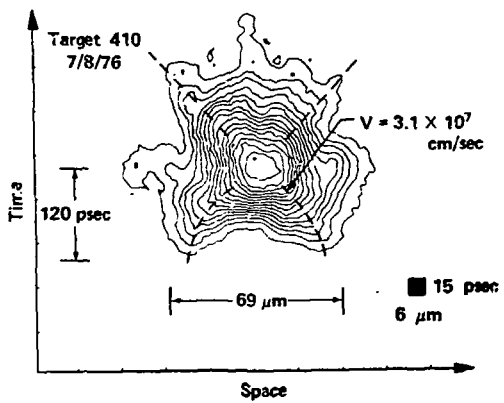

(b)

11/76

Fig. 9

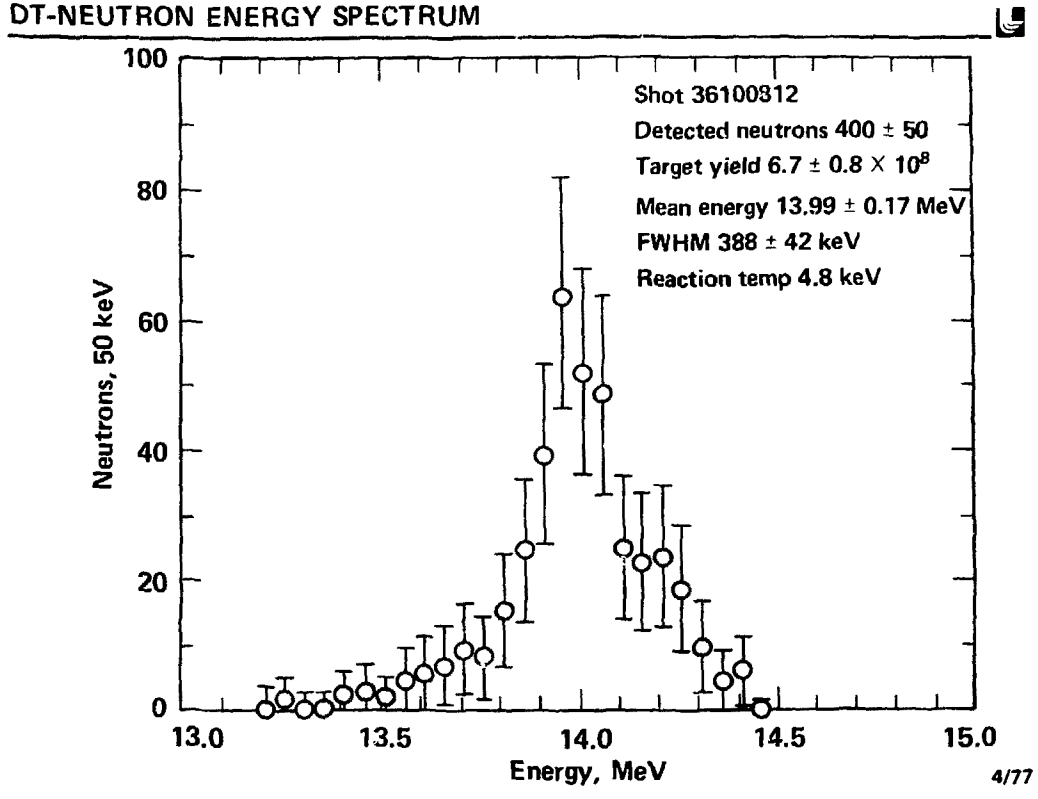
DT-NEUTRON ENERGY SPECTRUM
Shot 36100812
Detected neutrons 400 ± 50
Target yield 6.7 ± 0.8 X 10^8
Mean energy 13.99 ± 0.17 MeV
FWHM 388 ± 42 keV
Reaction temp 4.8 keV
Neutrons, 50 keV
Energy, MeV
100
80
60
40
20
0
13.0
13.5
14.0
14.5
15.0
4/77

Fig. 10

Image Reconstruction In Higher Order

Zone plate alpha imaging results:

Laser irradiated target

Coded image

Shot parameters

Power on target	:	2.4×10^{12} watt
Pulse width	:	$5\Omega \times 10^{-12}$ sec
D-T fill	:	1.6 mg/cm^3
Neutron yield	:	3×10^8
Ball diameter	:	86 μm

11 μm

7.4 μm

Reconstructed image
first order
$\delta \approx 10\ \mu$m

Reconstructed image
third order
$\delta \approx 3\ \mu$m

40-90-1177-2904

Fig. 11